journal

J. Am. Ceram. Soc., 1–9 (2011)
DOI: 10.1111/j.1551-2916.2011.04773.x

In situ Particle Generation and Splat Formation During Solution Precursor Plasma Spraying of Yttria-Stabilized Zirconia Coatings

Sivakumar Govindarajan,[‡] Rajiv Onkar Dusane,[§] and Shrikant Vishwanath Joshi[‡,†]

[‡]International Advanced Research Center for Powder Metallurgy and New Materials, Balapur, Hyderabad, India

[§]Department of Metallurgical Engineering & Materials Science, Indian Institute of Technology, Powai, Mumbai, India

Thermal barrier coatings (TBCs) based on Yttria-stabilized Zirconia (YSZ) deposited by the solution precursor plasma spray (SPPS) technique have been claimed to exhibit superior durability compared to conventional plasma spraying and even electron-beam physical vapor deposition. This has been attributed to the interesting features, like vertical cracks, nanosized pores, and fine splats that are inherent to SPPS-deposited YSZ coatings. However, the mechanism of coating formation during SPPS processing is not yet well understood. This study is aimed at understanding the influence of some key SPPS process variables on *in situ* generated particles and subsequent splat formation to augment the current level of understanding. The plasma power employed was found to play a major role in governing the morphology and phase constitution of *in situ* generated particles. The shape and size of the YSZ splats were also significantly influenced by the plasma power, but the substrate pre-heat was also noted to be a major determining factor. It was further observed that the SPPS typically involved *in situ* generation of very fine particulates (50–500 nm) and splats (typically 200–2000 nm), which lead to its nano-porous and homogeneous microstructure. The YSZ coating characteristics were also found to correlate well with the above results.

I. Introduction

Thermal barrier coatings (TBCs) developed employing solution precursor plasma spray (SPSS) technique have gained considerable research interest in recent times due to the inherent advantages that this route offers over conventional powder-based atmospheric plasma-sprayed coatings.[1–3] Yttria-stabilized Zirconia (YSZ) has been the most widely studied SPPS coating and has been shown to possess interesting intrinsic features, like vertical cracks, homogenous porosity, fine splats, etc. as well as greater durability under thermal cycling conditions.[2–4] In addition to the studies related to YSZ, few reports on deposition of TiO_2[5–6] and other functional coatings[7–8] have also been reported, with the possibility of the SPPS route obviating the need for expensive spray-grade powders also being a major attraction. As in the case of other thermal spray techniques, the SPPS coating characteristics are also significantly influenced by process parameters, such as plasma power, spray distance, precursor flow rate, substrate pre-heat, precursor characteristics, etc. However, the mechanism of coating formation during SPPS processing is not yet well understood.

The various reported studies on SPPS YSZ coatings have included presentation of a plausible deposition mechanism by Bhatia *et al*.,[9] involving breakup of atomized precursor droplets, followed by precipitation, gelation, pyrolysis, and sintering. This study providing first insight into the SPPS process was accomplished through careful experimentation, including sample extraction on glass slides and deposition of single-layer, as well as, thick coatings. Modeling of plasma interactions with precursor droplets to explain the formation of precipitates/particles[10–11] has also been carried out in an effort to explain the SPPS process. Yet other efforts have been aimed at predicting the influence of processing conditions on porosity, deposition efficiency, and thickness profiles in case of SPPS.[12–13] Chen *et al*.[6] have highlighted the importance of plasma power in controlling the phase transformations in SPPS TiO_2 coatings. In another study, although the starting precursor concentration was found to have no effect on the phase constitution of the coating, the splat formation and microstructural characteristics, particularly in terms of porosity were found to be significantly influenced.[14] The SPPS technique, being a rapid process involving various successive steps leading to coating formation within few milliseconds, is governed to a large extent by the *in situ* particle formation, which precedes melting of the particles and subsequent splat formation upon impact with the substrate resulting in coating formation. In related investigations on powder formation by spray pyrolysis and aerosol thermolysis, either hollow or solid particles have been reported to form, depending upon evaporation rate, ambient temperature, solute concentration, and droplet size.[15–16] It has been suggested that a key consideration in SPPS should be ideal to adopt process conditions that would promote volume precipitation within the entire volume of the fragmented droplet so as to result in well-defined solid particles to eventually obtain improved coating characteristics.[14]

Splat morphologies have been widely studied to provide basic information regarding the state of sprayed particles at impact in case of conventional powder-based plasma spray processes.[17–18] This approach has also been utilized in a few SPPS studies related to YSZ and TiO_2 coatings through collection of splats, as well as, by conducting single-scan spray experiments.[5–6,14] Such splat formation studies, coupled with investigation of *in situ* particle formation, can provide a good overall understanding of the SPPS process. However, the in-flight diagnostic tools that have been used with substantial success in case of various thermal spray processes, like plasma, HVOF, and cold gas dynamic spraying,[17,19–20] involving micrometer-sized powder particles cannot be used with SPPS process due to the typically fine size (~1 μm) of droplets/particles associated with the latter. Hence, developing a good understanding of the process is possible only through a thorough investigation of particles collected in-flight and a study of the splat morphologies.[1,5,14] In view of the above, the present study aims at understanding the influence of some key SPPS process variables on *in situ* powder formation and their subsequent melting in-flight. An attempt is also made to correlate findings from the above studies with properties of the SPPS-deposited coatings.

K. Faber—contributing editor

Manuscript No. 29529. Received March 30, 2011; approved June 30, 2011.
[†]Author to whom correspondence should be addressed. e-mail: svjoshi@arci.res.in

II. Experimental Procedure

(1) Precursor Preparation

The precursor solution used for the present study was prepared by mixing zirconium acetate [$Zr(C_2H_4O_2)_4$], diluted in acetic acid with an appropriate stoichiometric amount of yttrium nitrate hexahydrate [$Y(NO_3)_3.6H_2O$] (both procured from Sigma Aldrich, Munich, Germany) to ensure that their relative contents are adequate to produce 8 wt% yttria-stabilized zirconia. The solution was mixed with continuous magnetic stirring to ensure homogeneity. It is pertinent to point out that the choice of zirconia forming precursors is usually limited to zirconium alkoxides, zirconium oxychloride, or zirconium acetate. In general, alkoxides of yttrium and zirconium are highly moisture sensitive and readily form precipitates upon exposure to environment, while chlorides are known to produce harmful fumes, and thus, their use is avoidable.[21] Hence, zirconium acetate was chosen; its ability to dissolve in water to form an aqueous solution and the exothermic reaction resulting from the carbonaceous species were considered to be an added benefit. Yttrium acetate, yttrium isopropoxide, and yttrium nitrate have been used as yttria-forming precursors in prior studies. Apart from the relatively lower cost of yttrium nitrate compared to yttrium acetate, one additional factor that dictated the choice of the former was the fact that Y_2O_3 forms at a relatively lower temperature of 450°C when yttrium nitrate is used, whereas complete transformation of yttrium acetate to Y_2O_3 occurs only at 650°C.[22]

(2) Solution Precursor Plasma Spraying

Solution precursor plasma spraying was carried out using a robotic plasma spray system (Model 9MB; Sulzer Metco AG, Wohlen, Switzerland) equipped with a liquid delivery unit (Model SPS-II; Inframat Corporation, Manchester, CT). The SPPS process, schematically shown in Fig. 1, involves feeding of the liquid precursor into the plasma plume through an atomizing nozzle attached to the plasma gun. The plasma spraying parameters and injection conditions for the liquid feedstock are shown in Table I. The baseline plasma spray variables were set based on a previously reported study by Gell *et al.*[23] The plasma power was increased during experimentation by increasing the arc current, while maintaining the voltage constant at 70 V. The flow rate of primary gas was kept constant at 65 NLPM at 5.5 bar throughout, whereas the secondary gas flow rate was varied within a narrow window of 5.5–6.7 vol% (corresponding to 3.8–4.7 NLPM at 3.5 bar) to achieve the above voltage. The liquid injection conditions were kept constant throughout the present study regardless of the plasma power employed. However, it is pertinent to point out that previous work by Marchand *et al.*[24] provide interesting insights into the interactions between low-density feedstock droplets and a fluctuating plasma jet. A separate study on investigating the role of liquid injection parameters for a fixed set of plasma gun variables is presently ongoing in the authors' laboratory.

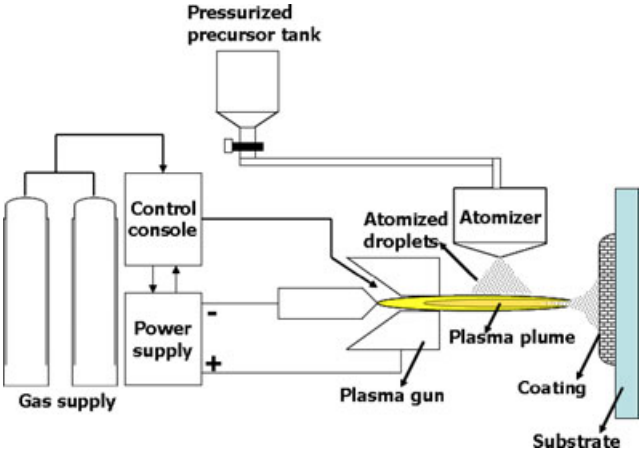

Fig. 1. Schematic of SPPS process.

Table I. Parameters Employed for Solution Precursor Plasma Spraying

	Parameters	Value
Plasma spray parameters	Operating gas	Ar, H_2
	Argon flow rate (NLPM) at 5.5 bar	65
	Plasma arc current (amp)	500–700
	Nozzle exit diameter (mm)	5.5
	Power (kW)	35–49
	Spraying distance (mm)	50
	Traverse speed (mm/s)	600
	Substrate pre-heat temperature (°C)	0–500
Injection parameters for liquid feedstock	Atomizing gas	Air
	Precursor feed rate (mL/min)	20
	Precursor injection depth (mm)	6
	Injection location from plasma torch exit (mm)	12
	Precursor tank pressure (bar)	2.8
	Atomization pressure (bar)	1.4

Particles generated *in situ* during the SPPS process were carefully collected in water rather than being allowed to impact a substrate and dried to enable their characterization. In a separate set of experiments, splats were collected on mirror-polished SS304 substrates pre-heated to varying temperatures by employing a high gun-traverse speed and allowing only few particles/droplets to pass through a shutter bearing a fine laser-drilled hole. For coating characterization studies, SS304 substrates were grit-blasted, ultrasonically cleaned, and preheated to varying extent, prior to coating deposition.

(3) Characterization of Precursor, In situ Formed Particles, Splats, and Coatings

A small quantity of the precursor solution prepared by mixing the zirconium acetate and yttrium nitrate salts, as specified in Section II(1), was dried on a hot plate and used for the TG/DTA analysis. Similarly, the *in situ* formed powder particles carefully collected in water were also thoroughly dried before thermal analysis. The starting YSZ precursor, as well as, the collected *in situ* formed particles were subjected to TGA analysis under oxygen atmosphere (Model STA 449F3; NETZSCH, Selb, Germany) to ascertain their thermal and crystallization behavior. The TG/DTA data were recorded up to a temperature of 1400°C for dried YSZ precursor, as well as, the collected particles at a heating rate of 10°C/min. The phases present in the collected particles and coatings were identified using an X-ray diffraction system (Model D8; Brukers AXS, Karlsruhe, Germany) and the average crystallite size was also estimated by applying the Scherrer formula. A field emission Scanning Electron Microscope (Model S43000SE/N; Hitachi, Tokyo, Japan) was used to examine the morphology of collected splats, as well as, the cross-sectional microstructural features of the coatings deposited. Prior to microstructural observation, the coated specimens were sectioned using a slow speed saw, and the cross-section mounted and polished. Microhardness values of the coatings were determined at 50 g load using a microhardness tester (Model VMH I04; Walter UHL, Asslar, Germany). The hardness values reported herein represent an average of 10 measurements made at different locations on each coated specimen.

III. Results and Discussion

(1) Precursor Characteristics

The progressive mass loss and heat flow curves obtained from TG/DTA analysis of the starting precursor solution, recorded at a heating rate of 10°C/min, are shown in Fig. 2. These curves reflect the successive evaporation of water, nitrates, acetates, and acetic acid manifested in the form of continuous loss in weight noted from the TGA curve. The likely sequence of events associated with the pyrolysis of YSZ precursor, based on data available in some prior reported studies,[25,26] is provided in Table II. Dehydration of the precursor occurs between 100°C and 220°C, which is followed by decomposition of acetate and acetic acid shown as a high amplitude exothermic peak between 220°C and 350°C. As reported by Samdi *et al*.,[25] amorphous zirconia transforms to black tetragonal zirconia, with the black color being due to some amount of carbon not eliminated following decomposition of acetates, as represented by a minor exothermic peak around 530°C. Similarly, the yttrium oxide formation is reported to occur around 480°C–530°C,[26] with the nitrate ions being removed around 500°C, represented by a minor endothermic peak as shown in Fig. 2. Upon heating to 900°C, the black tetragonal zirconia transforms into the white form, with the remnant carbon being eliminated to eventually stabilize the pure tetragonal zirconia phase.

(2) Analysis of In situ Formed Particles

(A) Morphology: The microstructure and associated intrinsic properties of thermally sprayed coatings, particularly the substrate-coating adhesion and the intersplat cohesion, are governed by the in-flight gas-particle transport phenomena and the dynamics of deformation of the impinging molten droplets on the virgin substrate, as well as, on a previously formed layer.[27] However, in case of SPPS coatings which involve a precursor solution rather than a spray-grade powder as the feedstock, an additional important criterion is the initial *in situ* transformation of the precursor salts into particles. Hence, the particle formation and its dependence on the spray parameters employed need to be well understood to develop any ability to reliably control the SPPS process.

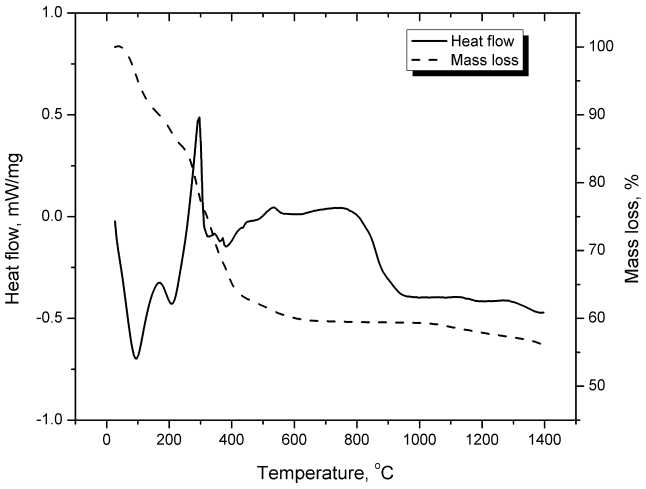

Fig. 2. TG/DTA curve for solution precursor used for depositing YSZ coatings.

Table II. Summary of Results from Thermogravimetric Analysis of Solution Precursor used for Depositing YSZ Coatings

Temperature (°C)	Gaseous release/phase formed	Thermal effect
100–220	H_2O	Endothermic
220–350	$(CH_3)_2CO + CO_2 + H_2O$	Exothermic
350–540	Nitrates, $CO_2 + H_2O$, amorphous ZrO_2, Y_2O_3	Endothermic and Exothermic
540–740	Black tetragonal ZrO_2	–
740–940	$CO_2 + H_2O$, White tetragonal ZrO_2	Exothermic

To study the *in situ* particle formation, the mid-stream plume "contents" were carefully collected in water and dried to enable characterization. The morphologies of the plume contents collected at different plasma power levels are shown in Fig. 3 and their analysis is extremely informative. With increase in power levels, the changes in morphology are clearly discernable. The morphology was found to vary significantly from the predominantly gel-like features noted at low plasma power of 35 kW to a preponderance of spherical particles observed at higher plasma power levels of 46 and 49 kW. Further analysis to ascertain the presence of any unpyrolyzed precursors in the plume contents collected midstream was also carried out and is discussed subsequently. As described by Bhatia *et al*.,[9] the presence of spherical particles at higher plasma power levels presumably corresponds to sintered YSZ particles. While the present study is restricted to investigating the influence of plasma power alone as an illustrative example, it is apt to comprehensively assess the role of other process variables, such as precursor concentration, flow rate, etc., as it would provide the necessary inputs to exercise desired control over the relative amounts of sintered spherical particles, unpyrolyzed particles, and gel-like features with remnant precursor at the moment of impact with the substrate. In this context, such unpyrolyzed particles and gel-like features have been reported to assist in the formation of vertical cracks and nano-pores in the SPPS TBCs, which eventually manifest in the form of enhanced durability.[2,28] The results from the present study also appear to support a previously reported effort which has shown that precursor injection in different regions of the plasma plume results in varied top surface morphologies.[2] In both cases, it is reasonable to assume that noted variations in surface morphology are attributable to different thermal exposure experienced by the precursor, either because of varying plasma power levels or because of differences in point of injection of the precursor droplets in a given plasma plume with a fixed gas temperature and gas velocity profile. It is also pertinent to note that the size of the *in situ* formed particles is typically less than 1 μm, with much finer particles being also evident particularly in Fig. 3(c). As discussed subsequently, this has an important bearing on the microstructure typical of SPPS coatings.

(B) Phase Constitution and Crystallite Size: The XRD phase analysis of the above particles is shown in Fig. 4 and clearly indicates the lack of crystallinity at lower plasma levels. Upon increase in plasma power, the peaks become sharper, indicating greater crystallinity in YSZ particles. In this context, it is relevant to mention that a previous study by Samdi *et al*.[25] has indeed identified formation of amorphous zirconia as an intermediate stage during pyrolysis of zirconium acetate + yttrium acetate precursors. At low power levels, presence of minor monoclinic and major tetragonal ZrO_2 peaks was noted, possibly on account of reduced yttria dissolution. However, at higher power levels, only tetragonal ZrO_2 peaks were seen. It is also to be noted that no free Y_2O_3 peaks were observed at any of the plasma power levels investigated. Scherrer's formula was used to estimate the crystallite size of *in situ* formed particles at different plasma power levels. At 35 kW power, it was found that the crystallite size was around 36 nm, which increased to 45 nm at 42 kW and 49 nm at 46 kW before dropping to 43 nm at 49 kW. It is pertinent to note that the YSZ particles

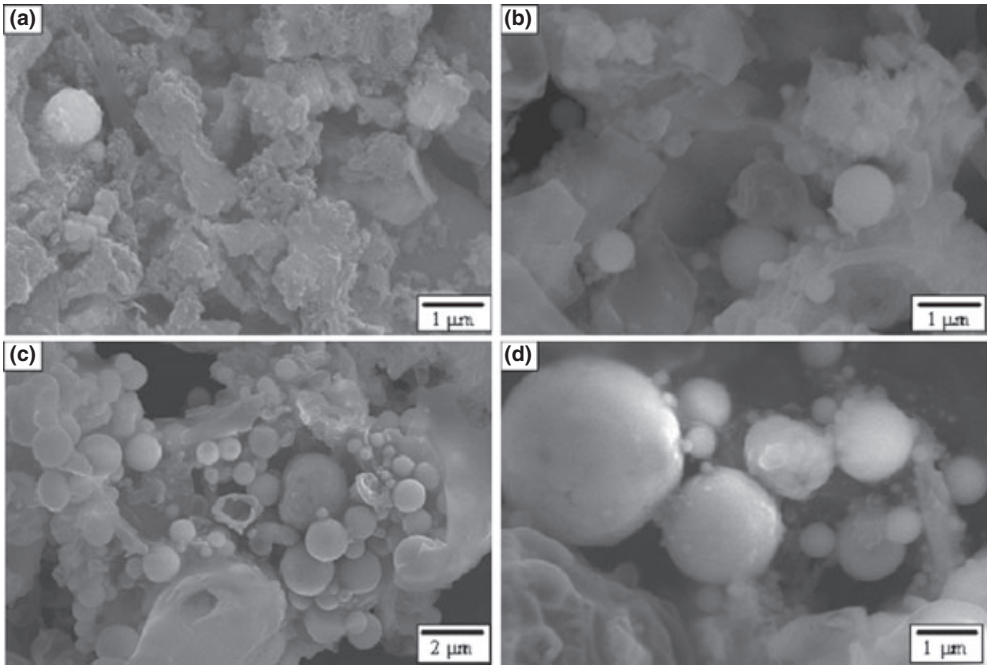

Fig. 3. Morphology of *in situ* formed particles collected at plasma power levels of (a) 35 kW, (b) 42 kW, (c) 46 kW, and (d) 49 kW.

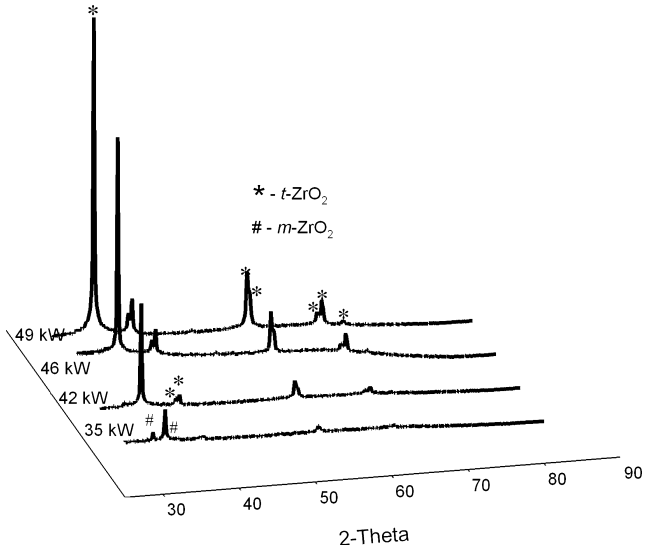

Fig. 4. Phase analysis of *in situ* formed particles collected at different plasma power levels.

exhibited nano-grained size, irrespective of the plasma power levels, similar to the trend observed in a previous study on SPPS TiO_2 coatings.[6]

(C) TG/DTA Analysis: The TG/DTA analysis was also carried out on the *in situ* formed particles collected at varying plasma power levels to assess their thermal behavior and derive information regarding the presence of any remnant unpyrolyzed matter along with the YSZ particles collected. Figure 5(a) clearly shows that the noted weight loss progressively decreases with increase in power level employed for collecting the *in situ* formed particles. This is consistent with the morphologies observed in Fig. 3 which, too, suggest that substantial unpyrolyzed mass is present at low plasma power levels but sharply reduces at higher power levels. As seen from Fig. 5(b), there is a constant endothermic peak in all cases at around 100°C, corresponding to removal of hydroxides. At around 300°C–400°C, which is close to the decomposition temperature of acetates and acetic acids from starting precursors as noted in Fig. 2, there is a clear indication of exothermic peaks for power levels up to 46 kW. The

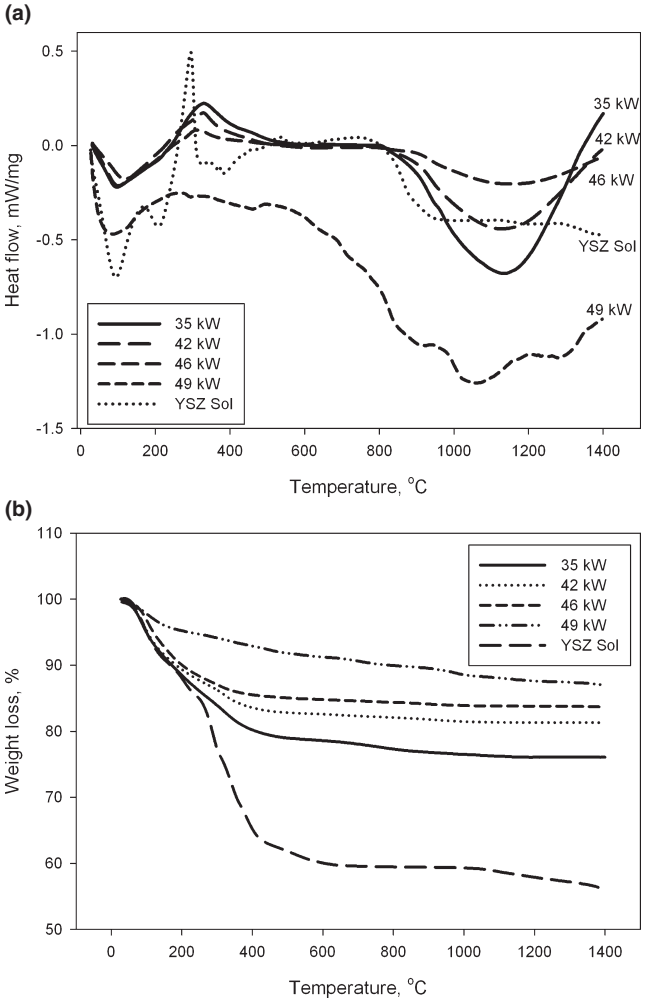

Fig. 5. TG/DTA analysis of *in situ* formed particles collected at different plasma power levels.

area under the curve of such exothermic peaks, which is a measure of heat release, monotonically reduces with increase in power levels until the peak virtually vanishes at the highest

plasma power of 49 kW, indicating completion of the pyrolysis action in-flight at such a high power level. At a temperature range between 1100°C and 1200°C, endothermic peaks of varying amplitudes decreasing with increase in plasma power can be observed. The above studies also suggest that lower plasma power levels similar to those used in conventional powder-based plasma spraying (35–40 kW) are clearly inadequate for producing the desired phase-pure solid YSZ particles from solution precursors. This is understandable due to the fact that additional energy is required to be provided to vaporize the solvents and other ligands, like acetates, nitrates, etc. present in precursor solutions.

To understand the changes in phase constitution that occur in the particles collected at different plasma power levels during the course of the TG/DTA analysis, XRD phase analysis was also done at the conclusion of the TG/DTA test. Results revealed that *in situ* formed particles collected at lower power levels transformed completely into tetragonal zirconia phase, as shown in Fig. 6. Surprisingly, in case of powders collected at higher power levels of 49 kW, higher monoclinic ZrO_2 phase (15%) was identified after TG/DTA analysis as compared to the 4% monoclinic ZrO_2 content determined in particles collected at 46 kW plasma power, plausible reason for which is discussed below.

Few prior studies have proposed a plausible mechanism for evolution of particles from the injected atomized precursor droplets.[11,15] It has been suggested that the solution droplet, upon contact with the high temperature, plasma plume gets heated up rapidly and starts evaporating from the surface. Initially, the solvents are removed upon high temperature exposure, leading to increase in solute concentration up to saturation level. Upon complete removal of solvents, either solid or hollow particles are formed depending upon the evaporation rate, solute concentration, etc., which are subsequently heated and accelerated to impact the substrate in molten/semi-molten state to form a coating. However, some amount of gel-like features have also been reported along with the solid/hollow particles, possibly as a consequence of interaction of the droplets being restricted to the periphery of the plasma plume, where the temperatures are relatively cooler.[2,9,13] It is logical to presume that reduction in plasma power has a similar effect and leads to greater retention of gel-like features, which are not only observed in the micrographs in Fig. 3(a), but also further supported by the greater weight loss in Fig. 5(b), as well as, the higher exothermic peaks observed around 400°C in Fig. 5(a). At high power levels, there is also a possibility of formation of hollow structures due to rapid surface solidification, along with solid particles formed under normal solidification rates (shown subsequently in Fig. 7) as described by Jayanthi *et al.*[15] Upon exposure to relatively higher temperatures, rapid evaporation of solvents leads to increased solute concentration near the surface, which induces the formation of hollow structures with some amount of retained precursor within. Previously reported droplet modeling studies focusing on SPPS[11] also corroborate that diffusive transport within the droplet is much slower than rapid increase in solute concentration through evaporation, leading to formation of a highly concentrated solution near the surface at higher plasma power levels. This thin shell of high solute concentration is likely to lead to the formation of a porous and/or impermeable layer, depending upon the concentration of solute and the resulting evaporation rates, with entrapped precursor solution inside. Rupture of hollow particles formed as a result of the above could be the source for the noted *m*-ZrO_2 peaks after TG/DTA analysis at high temperatures of 1400°C for particles collected at 49 kW power levels.

(3) Investigation of Splats

(A) Influence of Plasma Power: The physical status of particles at the point of impact with the substrate is a key factor influencing the microstructure of the coatings, as well as, its other characteristics. Conventional thermal spray literature is replete with studies involving careful collection of splats to develop an understanding of the particle condition at impact.[18,28] However, such studies in case of SPPS coatings have been surprisingly rare. In view of the above, the present study also included an investigation of splats collected on mirror-polished substrates pre-heated to different temperatures up to 500°C.

Typical splats, collected along the central axis of the plasma plume at different plasma power levels, are shown in Fig. 8. At lower plasma power levels, very few molten splats with spherical particles attached to irregular gel-like features were observed, as typified in Fig. 8(a). With increase in plasma power levels, the fraction of molten splats increases and the spherical particles progressively disappear, as the increasing thermal energy promotes reduced content of unpyrolyzed matter, as well as, subsequent melting of particles formed *in situ*. It is pertinent to note that, as the plasma power increases to about 46 kW, the shape of the molten splats attains the preferred disk-shaped feature as observed in Fig. 8(c). Usually, disk-shaped splats are preferred as they provide better contact with the surface than fragmented splats, thereby resulting in better adhesion–cohesion within the coating structure.[18,29] However, at further higher plasma power of 49 kW, significant splashing or disintegration of splats was observed, which could be a result of the *in situ* formation of hollow particles under high surface evaporation rates as previously discussed. As the molten hollow particles impact the substrate at T_{sub} = 500°C, the shell presumably

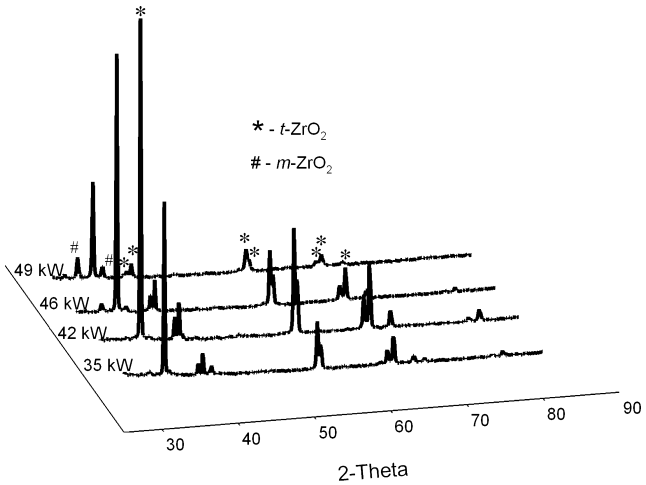

Fig. 6. Phase analysis after TG/DTA studies of *in situ* formed particles collected at different plasma power levels.

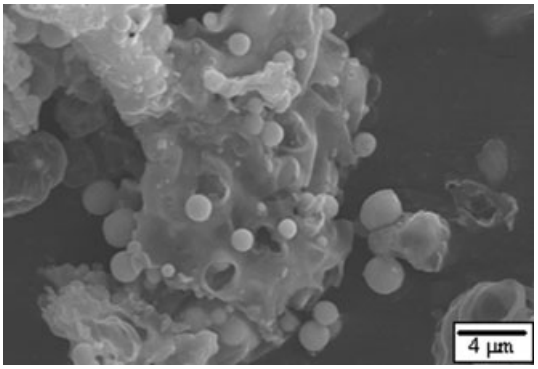

Fig. 7. Hollow and solid particle morphologies of YSZ particles at 49 kW.

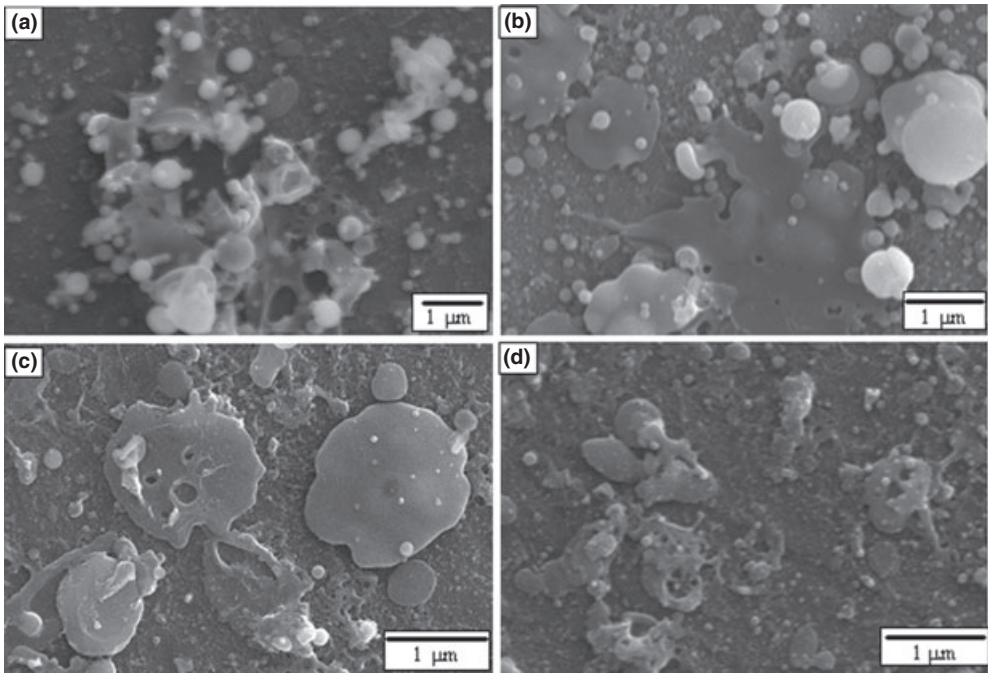

Fig. 8. Morphologies of splats collected on mirror-polished SS substrates pre-heated to 500°C at (a) 35 kW, (b) 42 kW, (c) 46 kW, and (d) 49 kW.

fractures to result in voids/pores within the flattened splat [as seen in Fig. 8(d)] and the precursor present within the shell undergoes evaporation, pyrolysis, etc. Similar observations were made by Chen *et al*.,[14] who reported solid/hollow particles being generated depending upon the precursor concentration, subsequently resulting in dense/porous coating microstructures.

There are also a couple of other interesting observations that can be made from the above study of splats. It is noted that the average sizes of splats is always less than 2 μm diameter, which is much smaller than the conventional plasma-sprayed YSZ splats that are in the size range of 50–100 μm.[18,29] Although fine-sized YSZ splats during SPPS spraying have been previously reported,[2,9,14] the above study demonstrates different splat morphologies under varied plasma power levels. Even when the plasma power level is slightly lower than that required for melting of particles after complete solvent evaporation as in Fig. 8(b), the size of the unmolten particulates is noted to be as fine as 50 nm or less, which results in some splats as small as 200–300 nm diameter at higher power levels, depicted in Figs. 8(c) and (d).

(C) Effect of Substrate Temperature: The influence of substrate temperature on splat morphology has been investigated through various studies in case of conventional plasma spraying with spray-grade powder feedstock for different coating-substrate temperature combinations.[18,30] The threshold substrate temperature for YSZ splats in conventional plasma spraying has been found to be around 100°C to yield the desired disk-shaped splats.[29] However, the same threshold may not hold in case of SPPS deposition due to the inherent differences in steps leading to coating formation, which may also involve impact of gel-like and/or partially pyrolyzed particulates onto the substrate. In appreciation of the above, experiments were specifically performed to ascertain the influence of substrate pre-heat temperature on splat formation. Based on the results ensuing from the previous studies discussed in Section III(2) above, a plasma power of 46 kW was utilized for all experiments. The resulting splats at varied substrate temperatures are shown in Fig. 9. The splat morphologies depicted clearly reveal that an increase in substrate pre-heat temperature is conducive to formation of more well-defined disk-shaped splats. In case of Fig. 9(a) with no substrate pre-heat, a significantly higher preponderance of very fine spherical particles is observed. Even at a substrate pre-heat temperature of 400°C [Fig. 9(c)], which is close to the decomposition temperature of the YSZ-forming precursor, minor amounts of gel-like features are visible in the splats. Hence, these splat formation studies suggest that, in addition to controlling the spray variables, like plasma power levels, the substrate should also be suitably pre-heated [Fig. 9(d)] to ensure good splat formation, and correspondingly, coatings of improved quality.

In the above context, it is relevant to note that appropriate control over the plasma spray variables and injection parameters for liquid feedstock needs to be exercised to manipulate the unpyrolyzed particles and gel-like features at the moment of impact with the substrate based on the coating system of interest. For example, as pointed out earlier, YSZ-based TBCs demand a porous microstructure with through-thickness vertical cracks for enhanced strain tolerance and longevity under thermal cycling conditions. The unpyrolyzed particles and gel-like features are known to influence the formation of vertical cracks and nano-pores in the SPPS TBCs[2,28] but may be undesirable for other coating systems that are designed to impart wear resistance, corrosion protection, etc.

(4) Correlating Coating Characteristics with In situ *Particle Generation and Splat Formation*

(A) Microstructure: Having gained some insight through the above studies on the influence of plasma power on *in situ* particle generation and the role of substrate temperature, as well as, plasma power in splat formation, attempt was also made to correlate the above to the characteristics of the resulting coatings. For this purpose, SPPS YSZ coatings were generated on stainless steel substrates sprayed with a detonation spray NiCoCrAlY bond coat. The cross-sectional microstructures of few selected SPPS coatings deposited under different conditions are shown in Fig. 10. The coatings generated at low plasma power of 35 kW but with substrate pre-heat to 500°C [Fig. 10(a)] and at high plasma power of 46 kW but with no pre-heat [Fig. 10(e)] exhibited relatively higher porosity and were accompanied by

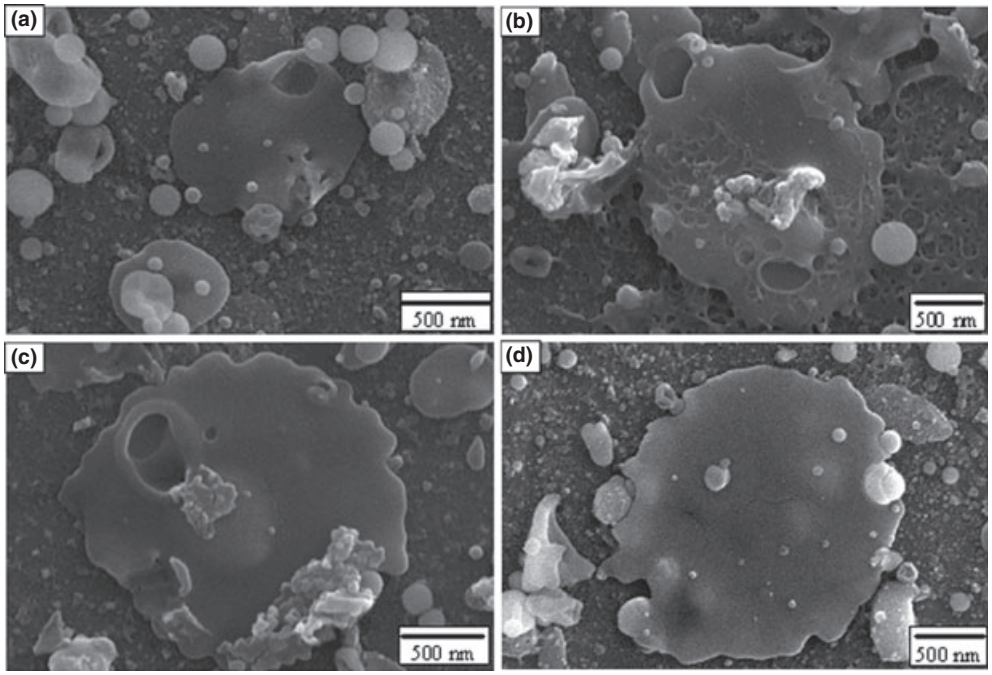

Fig. 9. Morphologies of splats collected on mirror-polished SS substrates at 46 kW plasma power with different pre-heat temperatures, (a) no pre-heat, (b) 200°C, (c) 400°C, and (d) 500°C.

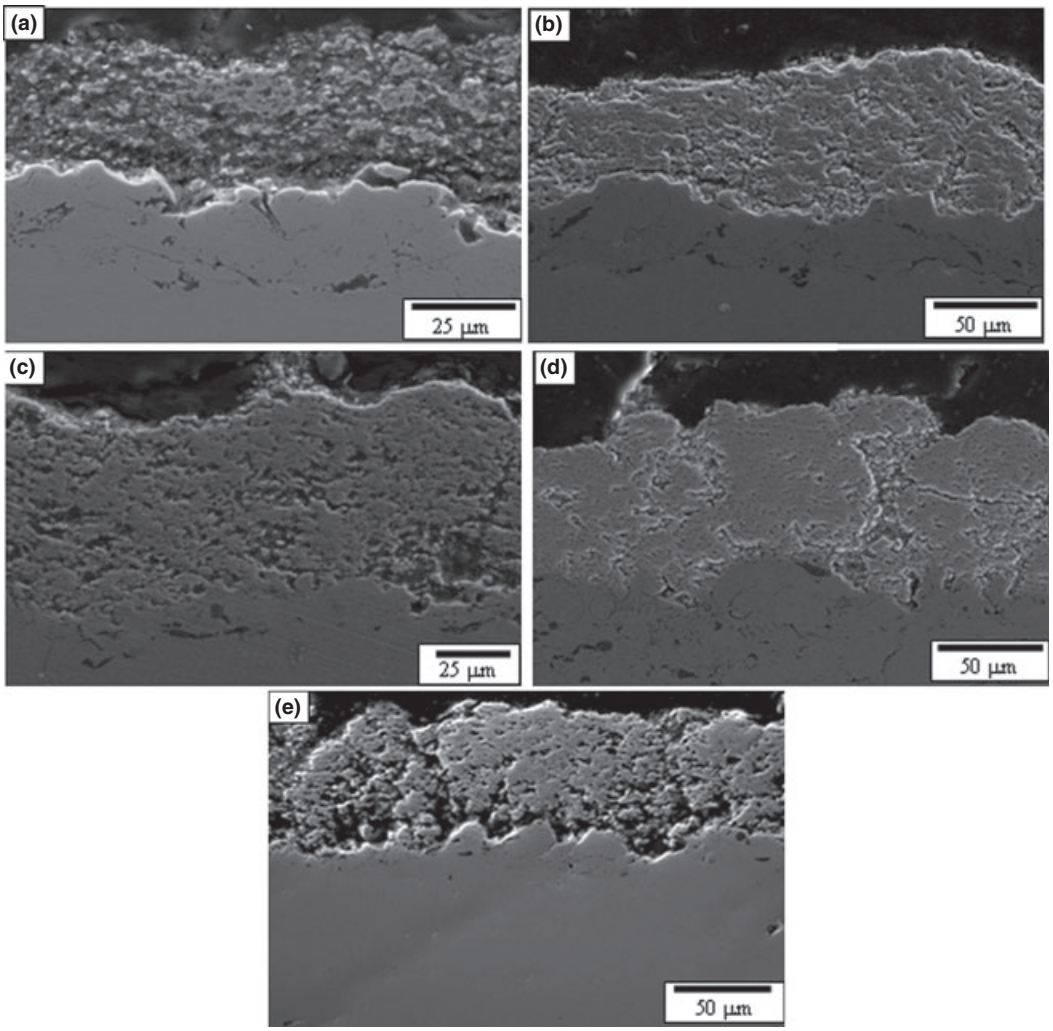

Fig. 10. Cross-sectional microstructure of SPPS YSZ coatings generated employing different deposition conditions, (a) Plasma power-35 kW with T_{sub}-500°C, (b) Plasma power-42 kW with T_{sub}-500°C, (c) Plasma power-46 kW with T_{sub}-500°C, (d) Plasma power-49 kW with T_{sub}-500°C, (e) Plasma power-46 kW with no pre-heat.

much lower deposition rates. This correlates well with the earlier findings which have shown that YSZ particle formation is not completed *in situ* at lower power levels and absence of substrate pre-heat precludes the formation of well-defined disk-shaped splats. In contrast, Figs. 10(b) and (c) corresponding to higher plasma powers of 42 and 46 kW, respectively, with substrate pre-heat to 500°C yielded relatively denser coatings. This is consistent with the increasing thermal energy promoting complete pyrolysis, as well as, subsequent melting of particles formed *in situ*. In the case of further higher plasma power of 49 kW included herein merely for the sake of comparison, regions of substantially dense microstructure but with multiple accompanying defects in the form of cracks and pores are evident. This is plausibly on account of the significant splashing or disintegration of splats noted earlier, resulting from the *in situ* formation of hollow particles under high surface evaporation rates and this, as discussed in the following section, manifests in the form of reduced hardness compared to coatings deposited at plasma powers of 42 and 46 kW.

(B) Porosity and Microhardness: Expectedly, this also has a bearing on the porosity and microhardness in the coated layer. Figure 11 illustrates the variation in microhardness as a function of plasma power. Consistent with the previously discussed results which have shown the *in situ* particle formation to be increasingly complete with increasing power level and the splats also to be well-defined as the plasma power is raised, the coating microhardness was found to increase substantially with plasma power up to 46 kW. Further increase in plasma power, however, led to coatings with reduced hardness, presumably on account of excess splashing and disintegration of splats for reasons discussed earlier. The microstructural features and microhardness obtained at different plasma powers seems to suggest that, for other conditions employed in this study (Table I), a minimum threshold plasma power of 42 kW with substrate preheat temperature of 500°C is essential to achieve relatively denser TBCs. This could plausibly be explained on the basis of splats observed in Fig. 8 which reveal that melting is very nearly complete at about 42 kW of plasma power.

(C) Phase Constitution: The XRD analysis of the above coatings was also carried out. Although the coatings were mainly constituted of the tetragonal ZrO_2 phase, some amount of monoclinic ZrO_2 phases could be seen at lower plasma power levels (4.5% at 35 kW). With increase in plasma power, the monoclinic ZrO_2 phase progressively reduced, and beyond 42 kW, tetragonal peaks alone were observed as shown in Fig. 12. To evaluate the yttria content in partially stabilized zirconia, the lattice parameters were initially estimated using the AIDS83 software (NIST, Gaithersburg, MD). Based on the lattice parameters determined, the $YO_{1.5}$ content in the coatings was estimated using the formula given by Scott.[31] The $YO_{1.5}$ content in the coatings at different plasma power levels was compared with the reference tetragonal ZrO_2 phase from ICDD database corresponding to JCPDF card no. 00-048-0224 and the results are shown in Fig. 13. The figure reveals that the completely stable tetragonal ZrO_2 phase is achieved when plasma power levels in excess of about 43 kW are adopted. This is consistent with the results obtained with the *in situ* collected particles as discussed earlier (see Fig. 4). Similarly, the crystallite sizes were also observed to increase with increase in plasma power and noted to be in the range of 35–46 nm, which closely matches the results obtained from *in situ* collected particle as discussed in Section III(2)(B). It is also pertinent to mention that crystallite sizes are in the range of 30–60 nm in case of YSZ and about 85 nm in case of TiO_2 coatings, have been reported in previous SPPS studies.[6,9]

IV. Conclusions

This article deals with a study of the influence of some key individual process parameters on SPPS coatings through a comprehensive investigation of *in situ* formed particles and splats to augment the current level of understanding of

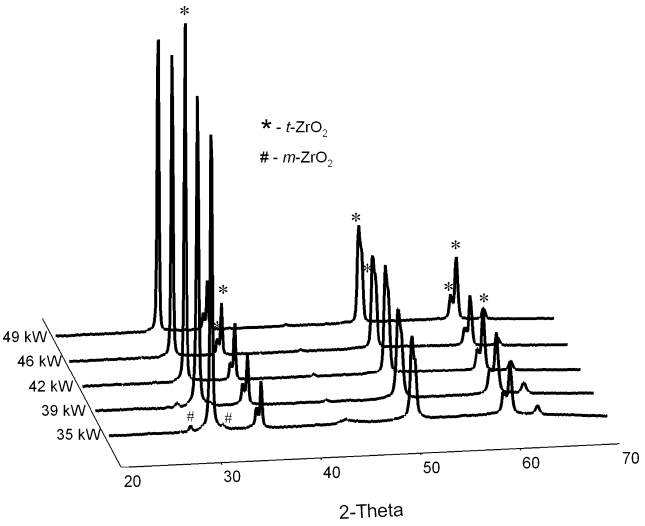

Fig. 12. Phase analysis of YSZ coatings generated at different plasma power levels.

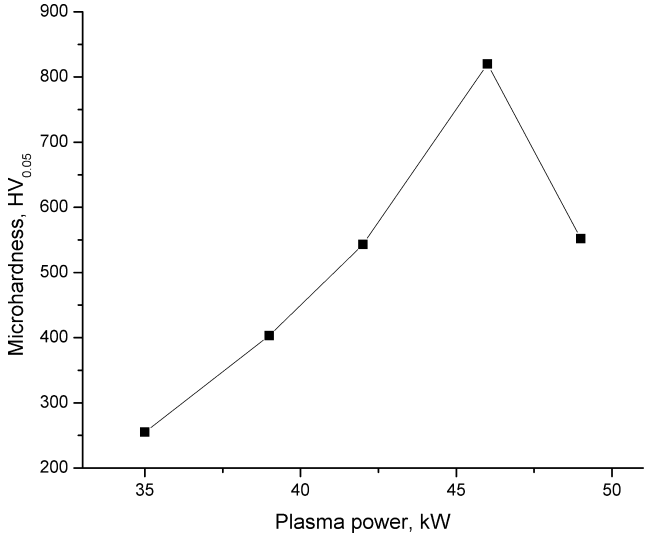

Fig. 11. YSZ coatings generated at different plasma power levels.

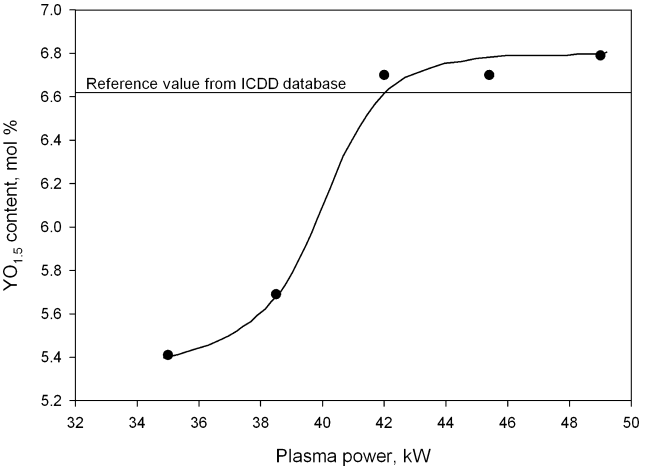

Fig. 13. Yttria content present in the tetragonal ZrO_2 phase for YSZ coatings generated at different plasma power levels.

deposition mechanisms associated with this relatively recent technique. The SPPS deposition of YSZ coating has been used as an illustrative case study. Plasma power levels were found to play a major role in determining the morphology and phase constitution of *in situ* generated particles. In addition, the shape and size of the YSZ splats were also noted to be significantly governed by the plasma power input. Based on the observed morphological features of the *in situ* formed particles and splats, a threshold plasma power of 46 kW was found to be essential to produce good YSZ coatings by the SPPS route. During the course of the study, it was further observed that the SPPS typically involved *in situ* generation of very fine particulates (typically 50–500 nm) and subsequent splats (200–2000 nm), which are responsible for its nano-porous and largely homogeneous microstructure. Investigation of splats revealed that the substrate temperature, too, was a major determining factor, with a substrate pre-heat to about 500°C yielding the desired splat morphologies. The characteristics of the YSZ coatings deposited at varying plasma power levels and substrate pre-heat conditions were found to correlate well with the above results pertaining to *in situ* generated particles and splat formation.

Acknowledgments

The authors thank Director, ARCI for his kind permission to publish this work. The support extended by Mr. A. Sathyanarayana, Mr. GVR. Reddy, Mr. L. Venkatesh, and Mr. K. Ramesh Reddy during experimental studies and characterization is gratefully acknowledged.

References

[1]P. Fauchais, R. Etchart-Salas, V. Rat, J. F. Coudert, N. Caron, and K. Wittmann-Teneze, "Parameters Controlling Liquid Plasma Spraying: Solutions, Sols, or Suspensions," *J. Therm. Spray Technol.*, **17** [1] 31–59 (2008).

[2]M. Gell, E. H. Jordan, M. Teicholz, B. M. Cetegen, N. P. Padture, L. Xie, D. Chen, X. Ma, and J. Roth, "Thermal Barrier Coatings Made by the Solution Precursor Plasma Spray Process," *J. Therm. Spray Technol.*, **17** [1] 124–35 (2008).

[3]P. Fauchais and G. Montavon, "Latest Developments in Suspension and Liquid Precursor Thermal Spraying," *J. Therm. Spray Technol.*, **19** [1–2] 226–39 (2010).

[4]N. P. Padture, K. W. Schlichting, T. Bhatia, A. Ozturk, B. Cetegen, E. H. Jordan, M. Gell, S. Jiang, T. D. Xiao, P. R. Strutt, E. Garcia, P. Mirazano, and M. I. Osendi, "Towards Durable Thermal Barrier Coatings With Novel Microstructures Deposited by Solution Precursor Plasma Spray," *Act. Mater.*, **49**, 2251–7 (2001).

[5]D. Chen, E. Jordan, M. Gell, and X. Ma, "Dense TiO_2 Coating Using the Solution Precursor Plasma Spray Process," *J. Am. Ceram. Soc.*, **91** [3] 865–72 (2008).

[6]D. Chen, E. Jordan, and M. Gell, "Porous TiO_2 Coating Using the Solution Precursor Plasma Spray Process," *Surf. Coat. Technol.*, **202**, 6113–9 (2008).

[7]V. Viswanathan, R. Filmalter, S. Patil, S. Deshpande, and S. Seal, "High-Temperature Oxidation Behavior of Solution Precursor Plasma Sprayed Nanoceria Coating on Martensitic Steels," *J. Am. Ceram. Soc.*, **90** [3] 870–7 (2007).

[8]B. G. Ravi, S. Sampath, R. Gambino, P. S. Devi, and J. B. Parise, "Plasma Spray Synthesis from Precursors: Progress, Issues and Considerations," *J. Therm. Spray Technol.*, **15**, 701–7 (2006).

[9]T. Bhatia, A. Ozturk, L. Xie, E. H. Jordan, B. K. Cetegen, M. Gell, X. Ma, and N. P. Padture, "Mechanisms of Ceramic Coating Deposition in Solution-Precursor Plasma Spray," *J. Mater. Res.*, **17** [9] 2363–72 (2002).

[10]A. Ozturk and B. M. Cetegen, "Modeling of Plasma Assisted Formation of Precipitates in Zirconium Containing Liquid Precursor Droplets," *Mater. Sci. Eng. A*, **384**, 331–51 (2004).

[11]S. Basu and B. M. Cetegen, "Modeling of Thermo-Physical Processes in Liquid Ceramic Precursor Droplets Injected into a Plasma jet," *Int. J. Heat Mass Trans.*, **50**, 3278–90 (2007).

[12]Y. Wang and T. W. Coyle, "Optimization of Solution Precursor Plasma Spray Process by Statistical Design of Experiment," *J. Therm. Spray Technol.*, **17** [5–6] 692–9 (2007).

[13]L. Xie, X. Ma, A. Ozturk, E. H. Jordan, N. P. Padture, B. M. Cetegen, D. T. Xiao, and M. Gell, "Processing Parameter Effects on Solution Precursor Plasma Spray Process Spray Patterns," *Surf. Coat. Technol.*, **183**, 51–61 (2004).

[14]D. Chen, E. H. Jordan, and M. Gell, "Effect of Solution Concentration on Splat Formation and Coating Microstructure Using the Solution Precursor Plasma Spray Process," *Surf. Coat. Technol.*, **202**, 2132–8 (2008).

[15]G. V. Jayanthi, S. C. Zhang, and G. L. Messing, "Modeling of Solid Particle Formation During Solution Aerosol Thermolysis: The Evaporation Stage," *J. Aerosol Sci. Technol.*, **19** [4] 478–90 (1993).

[16]S. Jain, D. J. Skamser, and T. T. Kodas, "Morphology of Single-Component Particles Produced by Spray Pyrolysis," *J. Aerosol Sci. Technol.*, **27** [5] 575–90 (1997).

[17]P. Fauchais, "Understanding Plasma Spraying," *J. Phy. D: Appl. Phys.*, **37**, 86–108 (2004).

[18]S. Sampath and X. Jiang, "Splat Formation and Microstructure Development During Plasma Spraying: Deposition Temperature Effects," *Mater. Sci. Eng. A*, **304–306**, 144–50 (2001).

[19]M. Gaona, R. S. Lima, and B. R. Marple, "Influence of Particle Temperature and Velocity on the Microstructure and Mechanical Behaviour of High Velocity oxy-Fuel (HVOF)-Sprayed Nanostructured Titania Coatings," *J. Mater. Process. Technol.*, **198**, 426–35 (2008).

[20]P. Sudharshan Phani, V. Vishnukanthan, S. V. Joshi, and G. Sundararajan, "Optical Diagnostics Study of Gas Particle Transport Phenomena in Cold Gas Dynamic Spraying and Comparison with Model Predictions," *J. Therm. Spray Technol.*, **17** [4] 551–63 (2008).

[21]R. M. Smith, X.-D. Zhou, W. Huebner, and H. U. Anderson, "Novel Yttrium-Stabilized Zirconia Polymeric Precursor for the Fabrication of Thin Films," *J. Mater. Res.*, **19** [9] 2708–13 (2004).

[22]H. M. Ismail and G. A. M. Hussein, "Texture Properties of Yttrium Oxides Generated from Different Inorganic Precursors," *Powd. Technol.*, **87**, 87–92 (1996).

[23]M. Gell, X. Ma, E. Jordan, N. P. Padture, L. Xie, D. Xiao, and A. DeCarmine, "Coatings, Materials, Articles and Methods of Making thereof"; US Patent No. 7,563,503B2, 2009.

[24]C. Marchand, C. Chazelas, G. Mariaux, and A. Vardelle, "Liquid Precursor Plasma Spraying: Modeling the Interactions Between the Transient Plasma Jet and the Droplets," *J. Therm. Spray Technol.*, **16** [5–6] 705–12 (2007).

[25]A. Samdi, B. Durand, M. Roubin, A. Daoudi, M. Taha, J. Paletto, and G. Fantozzi, "Pressing and Sintering Behaviour of Yttria Stabilized Zirconia Powders Prepared from Acetate Solutions," *J. Eur. Ceram. Soc.*, **12**, 353–60 (1993).

[26]A. E. Baranchikov, V. K. Ivanov, A. V. Dmitriev, E. A. Tkachenko, P. P. Fedorov, Yu. D. Tret'yakov, and V. V. Osiko, "Chemical Transformations of Basic Yttrium Nitrates During Ultrasonic–Hydrothermal Treatment," *Russ. J. Inorg. Chem.*, **51** [11] 1689–95 (2006).

[27]A. Kulkarni, A. Vaidya, A. Goland, S. Sampath, and H. Herman, "Processing Effects on Porosity-Property Correlations in Plasma Sprayed Yttria-Stabilized Zirconia Coatings," *Mater. Sci. Eng. A*, **359**, 100–11 (2003).

[28]L. Xie, D. Chen, E. H. Jordan, A. Ozturk, F. Wu, X. Ma, B. M. Cetegen, and M. Gell, "Formation of Vertical Cracks in Solution-Precursor Plasma-Sprayed Thermal Barrier Coatings," *Surf. Coat. Technol.*, **201**, 1058–64 (2006).

[29]L. Bianchi, A. C. Leger, M. Vardelle, A. Vardelle, and P. Fauchais, "Splat Formation and Cooling of Plasma-Sprayed Zirconia," *Thin Solid Films*, **305**, 35–47 (1997).

[30]A. Elsebaei, J. Heberlein, M. Elshaer, and A. Farouk, "Comparison of In-Flight Particle Properties, Splat Formation, and Coating Microstructure for Regular and Nano-YSZ Powders," *J. Therm. Spray Technol.*, **19** [1–2] 2–10 (2010).

[31]H. G. Scott, "Phase Relationships in the Zirconia-Yttria System," *J. Mater. Sci.*, **10**, 1527–35 (1975). □